Angewandte Chemie
Eine Zeitschrift der Gesellschaft Deutscher Chemiker

Supporting Information

German Edition: DOI:

Sampling of Glycan-Bound Conformers by the Anti-HIV Lectin *Oscillatoria agardhii* agglutinin in the Absence of Sugar**

*Marta G. Carneiro, Leonardus M. I. Koharudin, David Ban, T. Michael Sabo, Pablo Trigo-Mourino, Adam Mazur, Christian Griesinger, Angela M. Gronenborn, and Donghan Lee**

anie_201500213_sm_miscellaneous_information.pdf

Supplementary Methods

Sample preparation

OAA was expressed and purified as described in [2]. All NMR samples of free OAA contained 2 mM ^{15}N or ^{15}N, ^{13}C labeled OAA in 20 mM sodium acetate, 20 mM sodium chloride, 3 mM sodium azide, 90/10% H_2O/D_2O (pH 5) or 100% D_2O. Sugar-saturated OAA sample contained 1 mM ^{15}N labeled OAA in 20 mM sodium acetate, 20 mM sodium chloride, 3 mM sodium azide, 90/10% H_2O/D_2O (pH 5) and 12 mM of α3,α6-mannopentaose (Sigma-Aldrich). For measuring residual dipolar couplings (RDCs) partial alignment was induced by adding a mixture of N-octylpentaoxyethylene (C8E5) and octanol (r(C8E5/octanol) = 0.87; 5% C8E5/water)[17] to 500 μM of ^{15}N labeled OAA in 20 mM sodium acetate, 20 mM sodium chloride, 3 mM sodium azide, 90/10% H_2O/D_2O (pH 5).

NMR spectroscopy

Proton detected constant-time ^{15}N-CPMG relaxation dispersion experiments were recorded at 277 K on 800 MHz AVANCE III and 600 MHz AVANCE spectrometers equipped with 5-mm TCI cryogenic probes, as described in [18]. All the experiments were performed with a fixed delay time T_{CP} of 50 ms and variable CPMG frequencies ($\nu_{CPMG} = 1/(4\tau_{CP})$, where $2\tau_{CP}$ is the variable time delay between the 180° pulses during the CPMG element) of 80, 160, 240, 320, 400, 480, 560, 640, 720, 800, 880 and 960 Hz, with duplicated experiments recorded at 240, 480 and 720 Hz (600 MHz) and 240, 640 and 800 Hz (800 MHz) for error estimation. Besides, a reference spectrum for each data set was recorded, in which the relaxation delay is absent ($T_{CP} = 0$).

NMR data used for the structure determination of free OAA were collected at 298 K on 800 MHz AVANCE III (^{15}N-resolved [^1H,^1H] NOESY[19] (τ_m = 60 ms), $^{13}C_{aliphatic}$-resolved [^1H,^1H] NOESY[19] (τ_m = 80 ms), HNCA[19]), 700 MHz AVANCE III ($^{13}C_{aromatic}$-resolved [^1H,^1H] NOESY[19] (τ_m = 80 ms)) and 600 MHz AVANCE III (hCCH-TOCSY[19]) spectrometers equipped with 5-mm TCI cryogenic or 5-mm TXI room-temperature probes. In addition, backbone NH residual dipolar couplings were determined using IPAP-HSQC experiments[20] carried out on a ^{15}N-labeled isotropic sample and an aligned sample at 298 K on a 600 MHz AVANCE III spectrometer

equipped with a 5-mm TXI room-temperature probe, and a 700 MHz AVANCE spectrometer equipped with a 5-mm TCI cryogenic probe.

Three-bond $J(H^N H^\alpha)$ coupling constants were measured at 298 K on both free and sugar-saturated OAA on a 700 MHz AVANCE III spectrometer equipped with a 5-mm TXI room-temperature probe and a 800 MHz AVANCE III spectrometer equipped with a 5-mm TCI cryogenic probe using the approach described by Vuister and Bax[15].

All spectra were processed using NMRPipe[21] and analyzed with CARA.[22]

CPMG-RD data analysis

Peak intensities at each CPMG frequency were extracted using the model-based linear equation system implemented in the Computer Aided Resonance Assignment (CARA) application.[22] The effective transverse relaxation rate, R_2^{eff}, and associated uncertainties were calculated as described in [18] (and references therein). Nuclei that exhibited a difference in R_2^{eff} between the lowest and the highest implemented refocusing frequency larger than 2 s^{-1} were considered to display conformational exchange. The resulting dispersion profiles were fitted on a per residue basis to a two-state model using *ShereKhan*[23] both to the Bloch-McConnell model[24] (slow exchange) and to the Luz-Meiboom model[25] (fast exchange). The applicability of the slow exchange model over the fast exchange model was evaluated based on Akaike Information Criterion (AIC_C) differences ($\Delta AIC_C = AIC_{C,fast} - AIC_{C,slow}$).[26] Residues with $\Delta AIC_C > 10$ were fitted to the slow exchange model.

Assignment and structure determination

Backbone and side-chain ^1H, ^{15}N and ^{13}C resonances were assigned manually as described in [12]. All resonances with exception of the Y71 aromatic side-chain resonances and the carbonyl backbone resonance of W23 were assigned.[12] NOE cross-peaks were assigned using automated approaches (ATNOS/CANDID[27-28] module of UNIO'10 and CYANA 3.96[29]).

NOE derived distance constraints and residual dipolar coupling constraints were used as input for structure calculation. The presence of hydrogen bonds was evaluated based on initial structure calculations, and standard upper and lower distances for hydrogen bonds observed in more than 50% of the conformers were included in

subsequent runs. Structure calculations were performed with Xplor-NIH[30] using standard protocols, including a final energy minimization step with explicit solvent.
An ensemble of 20 structures with the lowest restraint violation energies was used to extract structural statistics on the ensemble using the PSVS 1.5 suite.[31]
The program MOLMOL[32] was used to analyze the structures and to prepare the structural representations in the figures.

$^3J(H^N,H^\alpha)$ analysis

The size of the $^3J(H^N,H^\alpha)$ couplings can be directly extracted from the intensity ratio between the cross and the diagonal peaks in a HNHA spectrum.[15] The experimental error was estimated using a Monte Carlo approach taking into account the signal-to-noise ratio (S/N) as error in the measured peak intensities. Likewise, the uncertainties associated with the $^3J(H^NH^\alpha)$ calculated based on angles measured from the X-ray structures were estimated using a Monte Carlo approach using the standard deviations of the Karplus coefficients from ref.[14].

Estimation of populations based on NOE ratios

Because the NOE intensity depends on the interatomic distance in a nonlinear fashion, populations cannot be estimated by directly comparing experimental NOE peak intensities with population weighted average distances. The intensity of a given NOE cross peak is inversely proportional to the sixth power of the distance between the atoms in question. Thus, the ratio of the sixth of the distances, d^{-6}, between two sets of two atoms (say, AB and CD) are directly comparable to the relative intensity, I, of the NOE peaks arising from each set of atoms:

$$\frac{d_{AB}^{-6}}{d_{CD}^{-6}} \approx \frac{I_{AB}^{Normalized}}{I_{CD}^{Normalized}}$$

with the NOE cross peak intensities I normalized to the corresponding NOE diagonal peak (i.e., $I_{ij}^{Normalized} = I_{ij}/I_{ii}$). Within this framework, experimental ratios can also be analyzed as a population weighted average of distance ratios. For a scenario with two limiting conformations, i.e. $p_A + p_B = 1$:

$$\frac{I_{AB}^{Normalized}}{I_{CD}^{Normalized}} \approx p_A \frac{d_{AB}^{-6}}{d_{CD}^{-6}} + p_B \frac{d_{A'B'}^{-6}}{d_{C'D'}^{-6}}$$

the populations can be estimated as:

$$p_A = \frac{I_{AB}^{Normalized}/I_{CD}^{Normalized} - d_{A'B'}^{-6}/d_{C'D'}^{-6}}{d_{AB}^{-6}/d_{CD}^{-6} - d_{A'B'}^{-6}/d_{C'D'}^{-6}}$$

$$p_B = 1 - p_A$$

Supplementary Tables

Table S1. Chemical shift differences (Δδ), exchange rates (k_{ex}) and populations (p_B) derived from CPMG relaxation dispersion experiments on sugar-free OAA at 277 K, extracted from resonances in slow exchange on the chemical shift time scale

Residue	Δδ (ppm)[a]	k_{ex} (s^{-1})	p_B (%)[b]
G11	− 4.02 ± 0.09	1075 ± 71	1.1 ± 0.1
S13	3.3 ± 0.2	1094 ± 173	0.5 ± 0.1
N18	1.5 ± 0.1	963 ± 29	1.6 ± 0.3
G26	+ 3.8 ± 0.5	40 ± 35	18 ± 16
S27	3.8 ± 0.2	72 ± 25	12 ± 4
R28	+ 2.8 ± 0.3	349 ± 259	3 ± 2
D30	2.3 ± 0.5	1185 ± 245	0.1 ± 0.2
Q31	+ 3.7 ± 0.2	109 ± 56	6 ± 3
N32	2.13 ± 0.05	314 ± 41	2.7 ± 0.4
M51	2.4 ± 0.4	165 ± 265	4 ± 7
G55	3.7 ± 0.4	91 ± 102	7 ± 8
N75	2.4 ± 0.1	378 ± 126	2.1 ± 0.7
W77	+ 6 ± 1	198 ± 501	6 ± 16
G78	3.2 ± 0.6	1622 ± 109	0.6 ± 3
W84	1.7 ± 0.1	471 ± 55	2.9 ± 0.6
G88	+ 1.38 ± 0.09	339 ± 42	3.2 ± 0.6
W90	3.4 ± 0.4	16 ± 13	17 ± 14
E96	4.0 ± 0.2	1235 ± 207	0.8 ± 0.2
Q98	2.7 ± 0.2	1223 ± 163	1 ± 0.3
N99	6.8 ± 0.4	1196 ± 339	1 ± 0.3
T117	1.4 ± 0.5	1174 ± 447	0.2 ± 0.3
G122	3.7 ± 0.6	88 ± 108	8 ± 10

[a] Residues for which the sign of the Δδ was determined by off-resonance R1ρ experiments are indicated with the corresponding sign.
[b] Dispersion curves were fitted to a two-state model, such that $p_A + p_B = 1$

Table S2. Summary of experimental constraints and structural statistics computed for the ensemble of 20 lowest energy structures of sugar-free OAA

Assignment Completeness (%)	99.9
NMR-derived constraints[a]	
Distance constraints	2419
Total NOE	2361
Intra-residue	175
Inter-residue	
Sequential (|i – j| = 1)	512
Medium range (|i – j| < 5)	278
Long range (|i – j| ≥ 5)	1396
H-bonds	58
Dipolar coupling constraints	89
$^{1}D_{NH}$	89
Structure statistics[a]	
Violations	
Distance constraints (> 0.5 Å)	0
RDC constraints (> 1.5 Hz)	0
R.m.s. deviations from idealized geometry	
Bond lengths (Å)	0.006
Bond angles (°)	0.621
Impropers (°)	1.003
Average pairwise r.m.s. deviation (Å)	
All Backbone atoms	0.7 ± 0.1
Backbone atoms in secondary structures [b]	0.33 ± 0.05
Procheck Ramachandran statistics[b]	
Most favored regions (%)	98.15
Additionally allowed regions (%)	1.69
Generously allowed regions (%)	0.08
Disallowed regions (%)	0.08

[a] Analyses were performed with PSVS version 1.5. [31] Average distance violations were calculated using the sum over r^{-6}.

[b] For residues in regular secondary structures (3-9, 18-24, 33-40, 46-53, 58-65, 70-76, 84-91, 100-106, 113-120, 126-132), calculated using DSSP.

Table S3. Interatomic distances[a] and NOE cross peak intensities used for estimating the populations of sugar-free and sugar-bound conformation in the absence of sugar for binding site 2[b] at 298 K

	Distance (Å)
Sugar-free	
H^N W77 - H^N G78	2.2
H^N G78 - H^N G79	2.9
H^N G78 – $H^{\alpha 2}$ G78	2.3
H^N G78 – $H^{\alpha 3}$ G78	2.9
Sugar bound	
H^N W77 - H^N G78	4.4
H^N G78 - H^N G79	2.1
H^N G78 – $H^{\alpha 2}$ G78	2.9
H^N G78 – $H^{\alpha 3}$ G78	2.3
NOE cross peak	**Intensity (a.u.)**
H^N W77 - H^N W77	254146
H^N G78 - H^N G78	594756
H^N G79 - H^N G79	1406681
H^N W77 - H^N G78	8079
H^N G79 - H^N G78	69809
H^N G78 – $H^{\alpha 2}$ G78	51290
H^N G78 – $H^{\alpha 3}$ G78	77531

[a] Measured from the sugar-free and sugar-bound X-ray structures. Hydrogen atoms were added to the original structures using Amber99sb force-field implemented in Gromacs.

[b] A similar analysis for binding site 1 is precluded by spectral overlap in the sugar-free NOESY spectrum and the presence of protein-protein contacts in the sugar-free crystal lattice.

Table S4. Dihedral angles ϕ and predicted[a] and measured $^3J(H^NH^\alpha)$ couplings for G11 (binding site 1) and G78 (binding site 2)

Binding site 1	
Sugar-free	
ϕ (°)	N/A[b]
Predicted $^3J(H^N,H^{\alpha2})$ (Hz)	N/A[b]
Measured $^3J(H^N,H^{\alpha2})$ (Hz)	Large (6.5 ± 0.5)
Predicted $^3J(H^N,H^{\alpha3})$ (Hz)	N/A[b]
Measured $^3J(H^N,H^{\alpha3})$ (Hz)	Small (4.7 ± 0.8)
Sugar-bound	
ϕ (°)	100.9
Predicted $^3J(H^N,H^{\alpha2})$ (Hz)	Large (9.2 ± 0.5)
Measured $^3J(H^N,H^{\alpha2})$ (Hz)	Large (8.1 ± 0.2)
Predicted $^3J(H^N,H^{\alpha3})$ (Hz)	Small (4.6 ± 0.4)
Measured $^3J(H^N,H^{\alpha3})$ (Hz)	Small (3.4 ± 0.6)
Binding site 2	
Sugar-free	
ϕ (°)	-89.7
Predicted $^3J(H^N,H^{\alpha2})$ (Hz)	Small (5.8 ± 0.4)
Measured $^3J(H^N,H^{\alpha2})$ (Hz)	Large (6.6 ± 0.5)
Predicted $^3J(H^N,H^{\alpha3})$ (Hz)	Large (8.0 ± 0.4)
Measured $^3J(H^N,H^{\alpha3})$ (Hz)	Small (4.9 ± 1)
Sugar-bound	
ϕ (°)	111.4
Predicted $^3J(H^N,H^{\alpha2})$ (Hz)	Large (9.8 ± 0.5)
Measured $^3J(H^N,H^{\alpha2})$ (Hz)	Large (8.0 ± 0.2)
Predicted $^3J(H^N,H^{\alpha3})$ (Hz)	Small (3.5 ± 0.4)
Measured $^3J(H^N,H^{\alpha3})$ (Hz)	Small (3.7 ± 0.6)

[a] Predicted based on the dihedral angles ϕ extracted from the sugar-free and -bound X-ray structures using the Karplus relationship[13] with coefficients suggested by Habeck et al. [14]

[b] Similar analysis for binding site 1 is precluded by the presence of protein-protein contacts in the crystal lattice.

Supplementary Figures

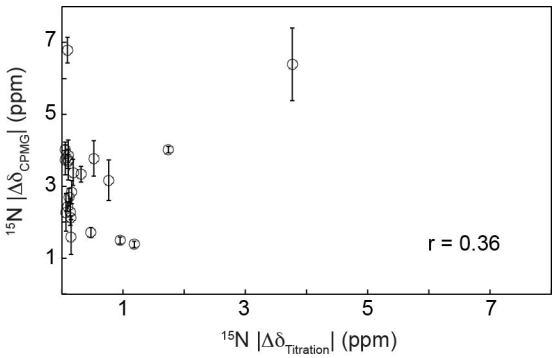

Figure S1. Comparison between backbone amide (^{15}N) chemical shift differences derived from CPMG relaxation dispersion experiments of residues exhibiting slow exchange on the chemical shift time scale ($\Delta\delta_{CPMG}$) and those extracted from sugar titration ($\Delta\delta_{Titration}$). The absence of any correlation between the chemical shift differences is highlighted by the Pearson correlation coefficient (r) of 0.36, indicating that the excited state conformation does not correspond to the sugar-bound conformation.

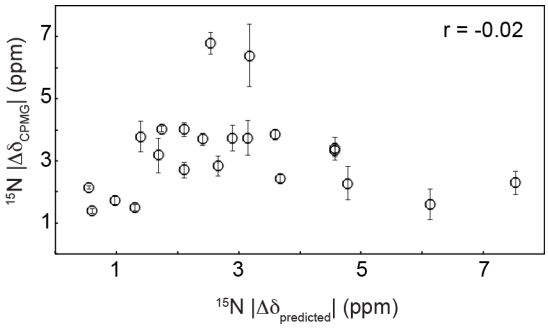

Figure S2. Comparison of backbone amide (^{15}N) chemical shift differences of residues in slow exchange on the chemical shift time scale derived from CPMG relaxation dispersion experiments ($\Delta\delta_{CPMG}$) and the chemical shift differences between the sugar-free native state and predicted random coil chemical shifts ($\Delta\delta_{predicted} = \delta_{1H\text{-}15N\ HSQC} - \delta_{random\ coil}$). Random coil chemical shifts were predicted with ncIDP [33]. The absence of a correlation between the chemical shift differences is highlighted by the Pearson correlation coefficient (r) of -0.02, indicating that the excited state conformation does not correspond to a random coil conformation.

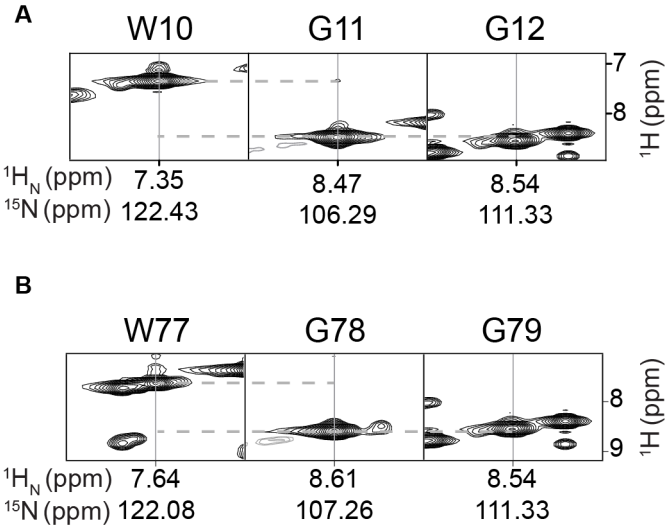

Figure S3. NOE cross peaks of sugar-saturated OAA agree with the sugar-bound conformation of the X-ray structures. The absence of NOE cross peak between H^N W10 and H^N G11 (binding site 1, **A**) and H^N W77 and H^N G78 (binding site 2, **B**) is in agreement with the much larger interatomic distance (4.4 Å) that is characteristic of the sugar-bound conformation in the X-ray structure.

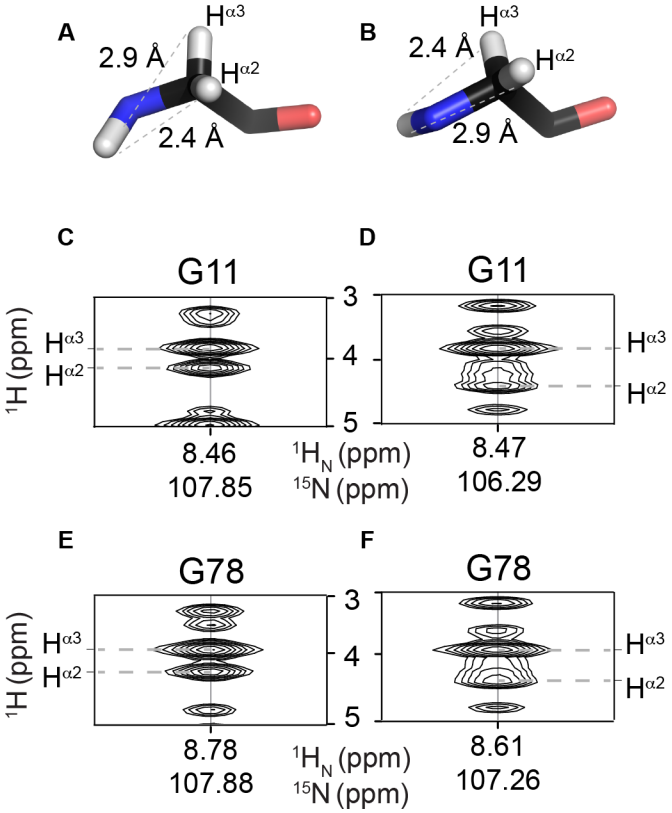

Figure S4. Stereospecific assignment for glycine H^{α} resonances. The interatomic distances between H^{N} and each H^{α} (**A** and **B** for the sugar-free and the sugar-bound conformations, respectively) compared to the relative intensities of the NOE cross peaks between H^{N} and each H^{α}. In the absence of sugar (**C** and **E** for binding site 1 and 2, respectively), the experimental data is best explained by the presence of both the sugar-free, **A**, and the sugar-bound, **B**, conformations. In the presence of sugar (**D** and **F** for binding site 1 and 2, respectively), the relative intensities of the NOE cross peaks are in good agreement with the distances extracted from the sugar-bound conformation, **B**, of the X-ray structure.

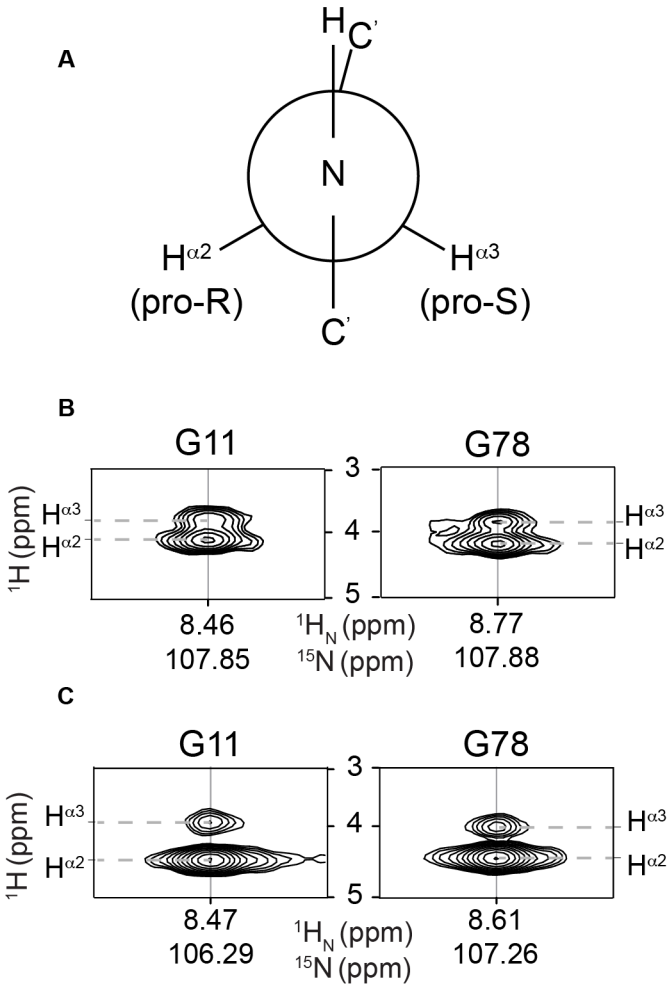

Figure S5. $^3J(H^N,H^\alpha)$ coupling constants suggest the presence of both sugar-free and -bound conformations in the sugar-free NMR solution structure. A, For glycines two $^3J(H^N,H^\alpha)$ couplings can be measure since two H^α atoms are present. The relative size of the two H^N - H^α cross peaks depends on the dihedral angle ϕ. In the absence of sugar, **B**, the experimental $^3J(H^N,H^\alpha)$ couplings suggest a conformational equilibrium between the sugar-free and -bound conformations, while for sugar-saturating conditions, **C**, the experimental $^3J(H^N,H^\alpha)$ couplings agree well with the $^3J(H^N,H^\alpha)$ coupling, predicted solely from the sugar-bound conformation of the X-ray structure.

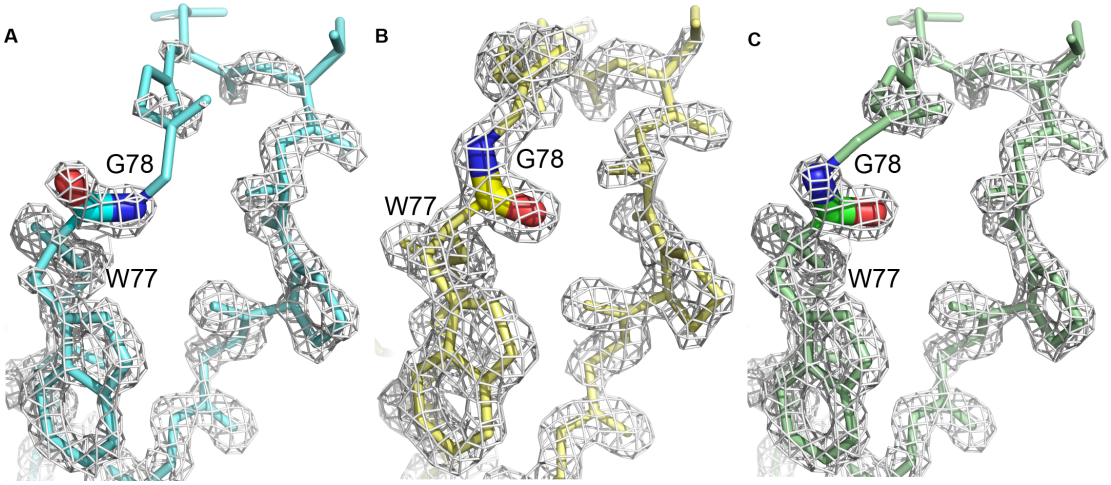

Figure S6. Electron density maps of OAA suggest flexibility in the absence of sugar in binding site 2. A X-ray structure and electron density map of binding site 2 in the absence of sugar (PDB code 3S5V). The weak electron density in the backbone region surrounding the peptide bond between W77 and G78 suggests static or motional disorder. **B** X-ray structure and electron density map of binding site 2 in complex with α3,α6 mannopentaose (PDB code 3S5X; the sugar is not shown for clarity). The clear electron density throughout the loop suggests that in the bound conformation the loop is in a predominant conformation. **C** A hybrid model, in which the peptide bond between W77 and G78 is flipped to mimic the bound conformation. Given the lack of electron density, this model fits also well into the electron density map of sugar-free OAA. The conformation of the peptide bond between W77 and G78 is highlighted in stick representation, with the backbone carbonyl and amide groups colored in red and blue, respectively.

Supplementary References

[17] M. Rückert, G. Otting, *J. Am. Chem. Soc.* **2000**, *122*, 7793-7797.

[18] D. Ban, A. Mazur, M. G. Carneiro, T. M. Sabo, K. Giller, L. I. Koharudin, S. Becker, A. Gronenborn, C. Griesinger, D. Lee, *J. Biomol. NMR* **2013**, *57*, 73-82.

[19] M. Sattler, J. Schleucher, C. Griesinger, *Prog. Nucl. Magn. Reson. Spectrosc.* **1999**, *34*, 93-158.

[20] M. Ottiger, F. Delaglio, A. Bax, *J. Magn. Reson.* **1998**, *131*, 373-378.

[21] F. Delaglio, S. Grzesiek, G. W. Vuister, G. Zhu, J. Pfeifer, A. Bax, *J. Biomol. NMR* **1995**, *6*, 277-293.

[22] R. L. J. Keller, *The computer aided resonance assignment tutorial*, CANTINA Verlag, **2004**.

[23] A. Mazur, B. Hammesfahr, C. Griesinger, D. Lee, M. Kollmar, *Bioinformatics* **2013**, *29*, 1819-1820.

[24] H. M. McConnell, *The Journal of Chemical Physics* **1958**, *28*, 430-431.

[25] Z. Luz, S. Meiboom, *J. Chem. Phys.* **1963**, *39*, 366-370.

[26] K. Burnham, D. Anderson, *Model selection and multimodel inference: a practical information-theoretic approach*, Springer, **2002**.

[27] T. Herrmann, P. Güntert, K. Wüthrich, *J. Mol.Biol* **2002**, *319*, 209-227.

[28] T. Herrmann, P. Güntert, K. Wüthrich, *J. Biomol. NMR* **2002**, *24*, 171-189.

[29] P. Güntert, C. Mumenthaler, K. Wüthrich, *J. Mol. Biol.* **1997**, *273*, 283-298.

[30] C. D. Schwieters, J. J. Kuszewski, N. Tjandra, G. Marius Clore, *J. Magn. Reson.* **2003**, *160*, 65-73.

[31] A. Bhattacharya, R. Tejero, G. T. Montelione, *Proteins: Struct., Funct., and Bioinf.* **2007**, *66*, 778-795.

[32] R. Koradi, M. Billeter, K. Wüthrich, *J. Mol. Graphics* **1996**, *14*, 51-55.

[33] K. Tamiola, B. Acar, F. A. A. Mulder, *J. Am. Chem. Soc.* **2010**, *132*, 18000-18003.